Analyst

ROYAL SOCIETY OF CHEMISTRY

PAPER

View Article Online
View Journal | View Issue

Cite this: *Analyst*, 2021, **146**, 2664

Ultrasensitive fluorometric biosensor based on Ti_3C_2 MXenes with Hg^{2+}-triggered exonuclease III-assisted recycling amplification

Liling Lu, Xiao Han, Jingwen Lin, Yingxin Zhang, Minghao Qiu, Ying Chen, Meijin Li * and Dianping Tang *

Received 28th January 2021,
Accepted 21st February 2021

DOI: 10.1039/d1an00178g

rsc.li/analyst

Herein a rapid and sensitive fluorometric bioanalysis platform for mercury(II) (Hg^{2+}) detection was innovatively developed using ultrathin two-dimensional MXenes (Ti_3C_2) as fluorescence quencher and Hg^{2+}-induced exonuclease III (Exo III)-assisted target recycling strategy for efficient signal amplification. Initially, fluorophore-labeled single-stranded DNA (FAM-labeled probe) can be easily adsorbed onto the surface of ultrathin Ti_3C_2 nanosheets by hydrogen bonding and metal chelating interaction, and the fluorescence signal emitted by the FAM-labeled probe is quenched strongly owing to the fluorescence resonance energy transfer between the FAM and ultrathin Ti_3C_2 nanosheets. Upon sensing the target Hg^{2+}, the protruding DNA fragment at the 3′ end of hairpin will hybridize with primer (hairpin-Hg^{2+}-primer), and then further digested by Exo III to produce a probe (nicker). The released target Hg^{2+} and primer continue to participate in the next recycling, resulting in more hairpin probes becoming nickers. The combination of a large number of nickers and FAM-probe resulted in a significant increase in the fluorescence signal of the system, which was attributed to the fact that the double helix DNA was more rigid and separated from the surface of the ultrathin Ti_3C_2 nanosheets. The obvious fluorescence signal change of the Ti_3C_2-based Exo III-assisted target recycling can be accurately monitored by fluorescence spectrometry, which is also proportional to the concentration of Hg^{2+}. Under optimum operating conditions, the peak intensity (520 nm wavelength) of fluorescence increased with increasing Hg^{2+} within a wide dynamic working range from 0.05 nM to 50 nM (R^2 = 0.9913) with a limit of detection down to 42.5 pM. The proposed strategy uses ultrathin MXenes as a platform for binding nucleic acids, which contributes to its potential in nucleic acid hybridization-based biosensing and/or nucleic acid signal amplification bio-applications.

Introduction

MXenes represent a new family of two-dimensional materials consisting of transition metal carbides and carbonitrides, which have attracted tremendous attention in the wider scientific community and industry due to their unique layered morphology, high conductivities, high surface area, excellent hydrophilicity, and environment-friendly properties.[1–3] Because of the excellent performance of this series, MXenes have been widely used in various fields, including but not limited to energy storage, photothermal, photo-/electrocatalysis, electromagnetic shielding, biosensors, and antibacterial agents.[4–8] MXenes have started to be considered as promising candidates for bio-applications and biosensor construction mainly due to their metallic conductivity, super-hydrophilic property (hydroxyl-terminated or oxygen surface) and operational biocompatibility (interact with biomolecules by hydrogen bonding, van der Waals force, electrostatic interaction, coordination bonds).[9–11] Recently, diverse protocols and strategies involving MXene materials have been reported in the field of analytical nanoscience/biosensing as well as biological nucleic acid nanopores. For instance, Zhang *et al.* reported an effective and universal self-standard ratiometric fluorescence resonance energy transfer (FRET) biosensing platform based on the fluorophore (Cy3)-labeled CD63 aptamer (high-affinity binding exosome nucleic acid sequence)/Ti_3C_2 MXenes for quantitative detection of exosomes.[9] In their work, Cy3-labeled single-stranded DNA (ssDNA) could be adsorbed on the surface of Ti_3C_2 MXenes through hydrogen bonding and chelating interactions between phosphate groups and Ti ions, causing intense fluorescence quenching. The combination of Cy3-labeled ssDNA and target exosomes caused a conformational change that dissociated on the surface of Ti_3C_2 MXenes, which resulted in a great recovery of Cy3 fluorescence.

Key Laboratory for Analytical Science of Food Safety and Biology (MOE & Fujian Province), State Key Laboratory of Photocatalysis on Energy and Environment, Department of Chemistry, Fuzhou University, Fuzhou 350116, P. R. China. E-mail: mjli@fzu.edu.cn, dianping.tang@fzu.edu.cn; Fax: +86 591 2286 6135; Tel: +86 591 2286 6125

Inspiringly, Pumera *et al.* elucidated the interaction of MXenes with fluorophore (FAM)-tagged ssDNA and double-stranded DNA (dsDNA), by means of fluorescence measurements and molecular dynamics simulations.[12] Therefore, MXenes exhibit high fluorescence quenching ability for fluorophore-labeled ssDNA and different affinities for ssDNA (strong adsorption) and dsDNA (weak adsorption), which make them play a huge role in nucleic acid-related biological fields.[13,14]

Enzyme-mediated target recycling and multiple-signal amplification strategies have been widely used in the field of nucleic acid-related nanoanalysis science to improve sensing sensitivity. Due to the powerful catalysis and high-efficiency digestion capabilities of enzymes, different kinds of enzyme-mediated biosensing of different signal transductions are widely used, including rolling circle amplification, strand-displacement amplification, isothermal exponential amplification reaction, polymerase chain reaction, *etc.*[15–18] These enzyme-driven strategies can continuously catalyze nucleic acid cleavage and/or polymerization reactions and are accompanied by multiple recoveries of target molecules, generating a large number of nucleic acid fragments to steadily improve the sensitivity of the system. However, the employment of primer and/or specific enzymatic recognition sequence requires very tight control of the bio-recognition and signal amplification in order to attain reproducible signal readout. In contrast, exonuclease III (Exo III) can stimulate its enzymatic activity without the need to recognize specific nucleic acid sequences and primer extensions.[19–21] It can continuously cut from the blunt end or 3′-recessed end of the DNA duplex in a short period to achieve the purpose of gradually removing single nucleotides. Therefore, Exo III can maintain its inherent sensitivity and high efficiency under simple and universal nuclease digestion, making it an indispensable presence in nucleic acid biosensing post-amplification.

Mercury (Hg^{2+}) environmental pollution causes serious toxicological damage to the human body (*e.g.*, nervous system damage, kidney damage, liver damage, brain damage, and various cognitive effects) due to its high toxicity and bioaccumulation/non-biodegradability through the ecological food chain.[22–24] Taking into account the high toxicity and huge health hazards of Hg^{2+}, the US Environmental Protection Agency and World Health Organization have set the maximum allowable concentration (threshold levels) of Hg^{2+} in drinking water as 10 nM and 30 nM, respectively. Consequently, accurate/reliable quantification, robustness, and instant detection of Hg^{2+} levels in common water quality is of great significance and urgently desired for global public safety and environmental pollution control. Toward this goal, herein we elaborately construct a powerful fluorometric platform for the quantitative screening of Hg^{2+} by using ultrathin two-dimensional MXenes (Ti_3C_2) as fluorescence quencher and Hg^{2+}-induced Exo III-assisted target recycling strategy for efficient signal amplification. In general, the method of analysis is achieved by the high fluorescence quenching ability and the different affinities for ssDNA (strong adsorption) and dsDNA (weak adsorption) by ultra-thin Ti_3C_2 MXenes (Scheme 1). Through the coordination chemistry interaction of thymine-Hg^{2+}-thymine (T-Hg^{2+}-T), the hairpin was partially hybridized with the primer to form a stable hairpin-Hg^{2+}-primer. Then, part of the hairpin (blue part) of the hairpin-Hg^{2+}-primer was continuously cut from the 3′-termini owing to the specific and excellent enzyme cleavage activity of Exo III, simultaneously releasing the primer, Hg^{2+}, and nicker (red part of hairpin). The free primers and Hg^{2+} digestion from the previous cycle are further combined with the remaining hairpins and the next round of signal amplification restarted to generate a large number of nickers. The resulting nicker and FAM-probe hybridize in a complementary manner to form a FAM-probe-nicker DNA duplex structure, which is far away from the MXene surface due to the rigid structure. In this case, the fluorescence signal is restored because the fluorophore is far away from the MXene surface, and the intensity of the restored fluorescence is positively correlated with the concentration of mercury ions.

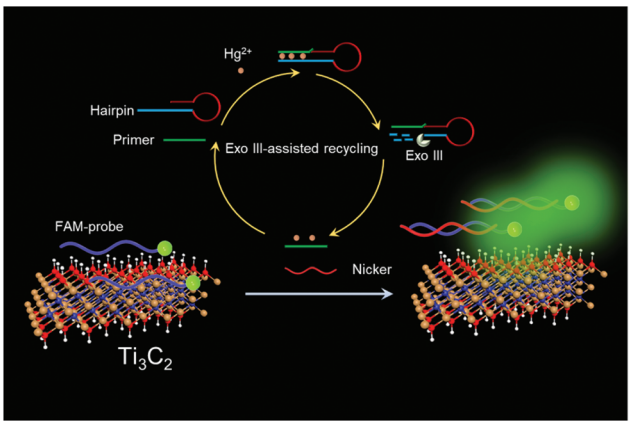

Scheme 1 Schematic illustration of the fluorometric biosensor for the detection of Hg^{2+} by using ultrathin two-dimensional MXenes (Ti_3C_2) as fluorescence quencher and Hg^{2+}-induced exonuclease III (Exo III)-assisted target recycling strategy for efficient signal amplification.

Experimental section

Chemicals and reagents

Aluminum titanium carbide powder (Ti_2AlC_3, 98%, 200 mesh) was purchased from Forsman Technology Co. Ltd. Hydrofluoric acid (HF, 40%, AR), Hg^{2+} standard sample, sodium phosphate monobasic dihydrate ($NaH_2PO_4{\cdot}2H_2O$, AR), sodium phosphate dibasic dodecahydrate ($Na_2HPO_4{\cdot}12H_2O$, AR, 99%), sodium chloride (NaCl, AR, 99.5%) and dimethyl sulfoxide (DMSO, AR, ≥99%) were obtained from Aladdin. All aqueous solutions in this experiment were prepared using deionized water (18.2 MΩ cm). All the HPLC-purified oligonucleotide sequences and Exo III (order no. B300061) were obtained from Sangon Biotech Co. Ltd. These sequences are listed as follows:

Primer: 5′-CTTTCTTCTTTGGCCCGG-3′

Hairpin: 5′-GTTTGTATGTTGGCCCGGACATACAAACTTTGTTGTTTG-3′

FAM-probe: 5′-FAM-CCGGGCCAACATACAAAC-3′

Preparation of Ti_3C_2 MXene nanosheets

As reported previously, Ti_3C_2 MXene nanosheets were synthesized by chemically etching Ti_3AlC_2 with HF aqueous solution.[9] Briefly, Ti_3AlC_2 powder (1.0 g) was slowly immersed in an HF aqueous solution (20 mL, 40%) at 45 °C along with magnetic stirring for 24 h to obtain a stable black suspension. To remove residual HF, the resulting black suspension was centrifuged (4000 rpm, 20 min) and washed with deionized water repeatedly until the pH value was greater than or equal to 6. Subsequently, HF-etched multilayered Ti_3C_2 powder (0.5 g) was mixed with DMSO (10 mL) and magnetically stirred for 24 h, followed by multiple centrifugations (3500 rpm, 5 min) and washing to collect the sediment. The collected precipitate was again mixed with deionized water (60 mL) and then sonicated in an ice water bath (temperature not exceeding 5 °C) for 1 h, accompanied by nitrogen bubbling to remove dissolved oxygen and prevent oxidation. After the ultrasonic treatment, the solution was centrifuged (3500 rpm, 1 h) and the dark supernatant (Ti_3C_2 colloidal solution) was collected and sealed for further characterization and experiment.

Fabrication of fluorometric biosensor platform and measurement

In a typical assay, FAM-probe (10 μM, 1 μL) and Ti_3C_2 MXene nanosheets (0.1 mg mL^{-1}, 49 μL) were mixed in phosphate-buffered saline (PBS; 10 mM, pH 7.4, 150 μL) to obtain FAM-probe/Ti_3C_2 biological probe. After incubating the above mixture for 10 min, the fluorescence emission spectrum was collected in the range of 500 to 650 nm at an excitation wavelength of 480 nm, and the fluorescence intensity peak (520 nm wavelength) was measured. For the Hg^{2+}-triggered Exo III-assisted recycling amplification process, primers (0.5 μM, 4 μL), hairpin (10 μM, 2 μL), Exo III (5 U), and Hg^{2+} standard sample (2 μL, final concentration range from 0 to 50 nM) were added in PBS (12 μL, 10 mM, pH 7.4, containing 1× Exo III buffer) and incubated at 37 °C for 100 min to perform the enzymatic reaction. Finally, the solution after the enzymatic reaction was heated at 70 °C for 20 min to completely inactivate Exo III, and then added to FAM-probe/Ti_3C_2 solution (180 μL) for fluorescence detection.

Results and discussion

Detailed characterization of Ti_3C_2 MXene nanosheets

In this work, ultrathin Ti_3C_2 nanosheets have high-efficiency fluorescence quenching capabilities and different affinities for ssDNA/dsDNA. For this reason, the successful synthesis of HF-etched and DMSO-intercalated Ti_3C_2 nanosheets is the core of the whole fluorometric biosensing system. The intrinsic microstructures and morphological evolution from Ti_3AlC_2 to Ti_3C_2 were investigated with scanning electron microscopy (SEM; JEOL JSM-7001F). Evident from the SEM image (Fig. 1A), the raw Ti_3AlC_2 exhibited a complete bulk structure with a smooth surface. The corresponding energy-dispersive X-ray spectroscopy (STEM-EDS) elemental mapping analysis of the raw

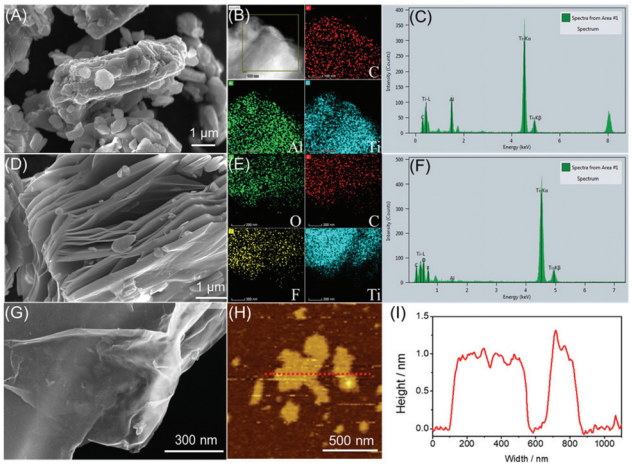

Fig. 1 (A) SEM image, (B and C) HAADF-STEM image and EDS element mapping/analysis of Ti_2AlC_3. (D) SEM image, (E and F) EDS element mapping/analysis of HF-treated Ti_3C_2. (G) SEM image and (H) AFM image of DMSO-intercalated and delaminated Ti_3C_2 (single layer and few layers). (I) Height distribution along the red line in (H).

Ti_3AlC_2 demonstrated the coexistence and nonlocalized distribution of C, Al, and Ti elements in the entire composite (Fig. 1B and C). After 24 h of etching of the aluminum layer by HF, the Ti_3C_2 layer showed a classic loosely stacked "accordion" structure (Fig. 1D). As expected, the elemental mapping images demonstrated the homogeneous distributions of O, C, F, and Ti elements over the entire architecture of Ti_3C_2 (Fig. 1E and F). Compared with the EDS spectrum before and after HF etching of Ti_3AlC_2 (Fig. 1C *vs.* Fig. 1F), the synergistic appearance of O and F element content and the sharp decrease of Al element content indicated that Ti_3C_2 was successfully obtained by HF etching. After DMSO intercalation and ultrasonic mechanical delamination treatment, it is easy to obtain ultrathin single-layer/few-layer monodisperse Ti_3C_2 nanosheet with a flat surface because of the weakened interlayer interactions (Fig. 1G). Beyond that, the thickness information of the Ti_3C_2 nanosheet was further verified by atomic force microscopy (AFM; Nanoscope, Bruker). The image in Fig. 1H illustrated that the Ti_3C_2 nanosheet is well distributed on the mica surface and presents a typical two-dimensional morphology with a size of several hundred nanometers. Along the red line in Fig. 1H, it can be seen that the Ti_3C_2 nanosheet has a height distribution of between 0.92 and 1.31 nm (Fig. 1I), which is very close to the theoretical value of a single layer (0.98 nm), indicating that the synthesized Ti_3C_2 nanosheet is a single layer.

To get an insight into the chemical valence states of surface atoms, X-ray photoelectron spectroscopy (XPS; ESCALAB 250) was further carried out. As shown in the XPS spectra of Fig. 2, the corresponding element valence states (Ti 2p, O 1s, F 1s and C 1s) can be observed in Ti_3C_2. Three individual peaks are situated at 684.71 eV, 685.34 eV and 453.0 eV (Fig. 2A), corresponding to C–Ti–F_x, $TiO_{2-x}F_x$ and byproducts (AlF_x) in Ti_3C_2, respectively. Similarly, the peaks situated at 454.8 eV (460.5

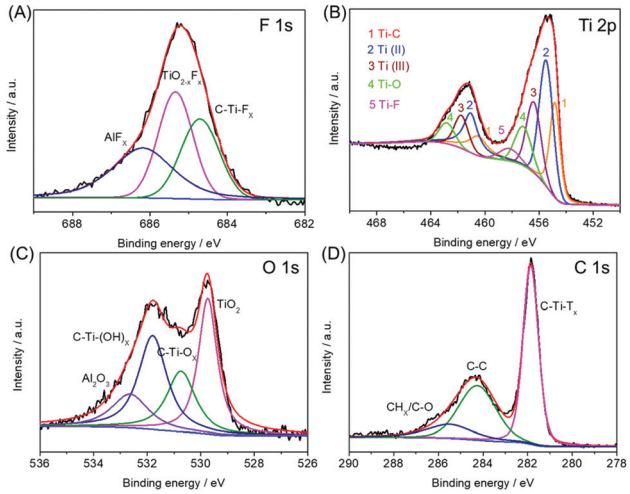

Fig. 2 High-resolution XPS spectra of (A) F 1s; (B) Ti 2p; (C) O 1s; and (D) C 1s.

eV), 455.48 eV (461.06 eV), 456.39 eV (461.75 eV), 457.16 eV (462.82 eV), and 458.19 eV (Fig. 2B), correspond to Ti–C, Ti^{2+}, Ti^{3+}, Ti–O and Ti–F, respectively. The binding energies of TiO_2, C–Ti–O_x, C–Ti–$(OH)_x$, and Al_2O_3 are 529.73 eV, 530.72 eV, 531.79 eV, and 532.64 eV (Fig. 2C). Besides, the C 1s spectrum of Ti_3C_2 was reasonably fitted with three peaks located at 281.86 eV, 284.25 eV and 285.5 eV (Fig. 2D), corresponding to C–Ti–T_x, C–C and C–H_x/C–O, respectively.[25] Based on the aforementioned results from SEM, AFM and XPS, we might conclude that ultrathin Ti_3C_2 nanosheets could be successfully synthesized *via* HF etching–DMSO intercalation–ultrasonic delamination.

Feasibility of Ti_3C_2-based Hg^{2+}-induced Exo III-assisted target recycling fluorometric system

In this work, the nickers released from the Hg^{2+}-induced Exo III-assisted target recycling system hybridized with FAM-probe to cause fluorescence recovery. To clarify this point, native polyacrylamide gel electrophoresis (PAGE, 8%, Fig. 3A) was used to verify whether the above strategy can be performed *via* the expected pathway. Two clear and bright bands (lanes A and B) corresponding to the hairpin and primer can be observed. After the hairpin reacted with Hg^{2+} and primer, a relatively low-mobility and well-defined band (lane C) appeared, mainly due to the production of hairpin-Hg^{2+}-primer with a larger molecular weight. After incubating Exo III with the system of lane C, the brightness of the band corresponding to lane C is significantly reduced due to enzyme digesting (lane D). More importantly, a new and high-mobility band appeared corresponding to a mixture of nicker and primer (note: nicker and primer were of the same number of bases). The PAGE analysis result clearly and powerfully illustrates that the Hg^{2+}-induced Exo III-assisted target recycling strategy can be executed in accordance with the proposed protocol process. Certainly, another inevitable question is whether the Hg^{2+}-induced Exo III-assisted target recycling system can be further employed for

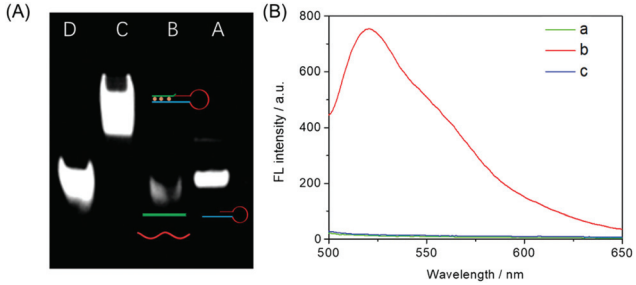

Fig. 3 (A) PAGE (8% gel) for different samples (lane A: hairpin; lane B: primer; lane C: hairpin + primer + Hg^{2+}; lane D: hairpin + primer + Hg^{2+} + Exo III). (B) Fluorescence spectra of (a) Ti_3C_2 + FAM-probe, (b) Ti_3C_2 + FAM-probe + hairpin + primer + Hg^{2+} + Exo III, and (c) Ti_3C_2 + FAM-probe + hairpin + primer + Exo III.

fluorescence sensing and detection. In this regard, fluorescence emission spectra were applied to monitor the state of different control experiments (Fig. 3B). After simply mixing FAM-probe and Ti_3C_2, almost no fluorescence is observed (curve a). The above phenomenon can be attributed to the fluorescence quenching caused by FRET when FAM-probe is adsorbed on the Ti_3C_2 surface. After reacting FAM-probe/Ti_3C_2 with hairpin, primer, Exo III and Hg^{2+} (50 nM), significant fluorescence enhancement is observed (curve b), attributed to the weak affinity of Ti_3C_2 to FAM-probe-nicker rigid DNA duplex. For comparison, the fluorescence behavior in the absence of Hg^{2+} is not significantly different from that of FAM-probe/Ti_3C_2 (curve c). These results revealed that the Ti_3C_2-based Hg^{2+}-induced Exo III-assisted target recycling system is triggered in the presence of Hg^{2+} and can be used for the determination of target Hg^{2+} *via* fluorescence.

Optimization of experimental conditions

To obtain better measurement performance, the concentration of Exo III and the reaction time of the whole system (including hairpin-Hg^{2+}-primer formation, Exo III digestion time and FAM-probe-nicker formation) were carefully optimized through variable control methods. This involved performing multiple rounds of experiments at a constant Hg^{2+}concentration (50 nM), and recording the changes in peak fluorescence intensity (520 nm wavelength) for comparison. Generally, the cleavage efficiency of hairpin-Hg^{2+}-primer depends on the amount of Exo III, which further affects the number of nickers produced. In this regard, the concentration of Exo III is the key to restrict the entire biosensing system. The peak fluorescence intensity increases rapidly with the concentration of Exo III, and reaches a plateau at 5 U (Fig. 4A). The introduction of a high concentration of Exo III did not significantly increase the peak fluorescence intensity of the system. Therefore, 5 U Exo III was used as an optimized parameter in subsequent experiments. By the same token, we further optimized the reaction time of the sensing platform, including Hg^{2+}-induced Exo III-assisted target recycling and fluorescence recovery. Similarly, the fluorescence intensity of the system continues to increase with the

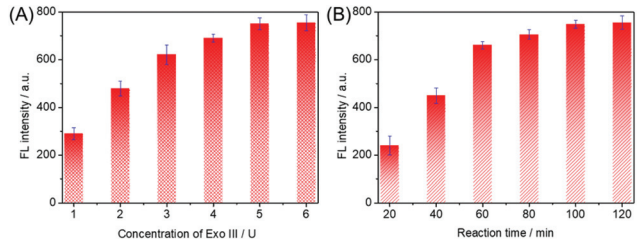

Fig. 4 Influence of (A) Exo III concentration and (B) incubation time of Ti_3C_2-based Hg^{2+}-induced Exo III-assisted target recycling on peak fluorescence intensity (520 nm wavelength) of the fluorometric aptasensing platform by using 50 nM Hg^{2+} as an example.

reaction time and the optimal reaction time was obtained within 100 min for subsequent experiments (Fig. 4B).

Dose responses of the fluorometric system toward target Hg^{2+}

By coupling Hg^{2+}-induced Exo III-assisted target recycling with the FAM-probe/Ti_3C_2 biological probe, different levels of Hg^{2+} (0 to 50 nM) were systematically detected under the optimized conditions. As the concentration of Hg^{2+} increased successively, the fluorescence intensities obviously recovered until reaching a plateau, indicating more FAM-probe-nicker away from the Ti_3C_2 surface. A good linear dependence of fluorescence intensity-Hg^{2+} concentration curves was obtained (Fig. 5A) with the correlation equation expressed as y (fluorescence intensities at 520 nm) = 221.1 × log $C_{[Hg^{2+}]}$ + 352.81 (nM) (correlation coefficient R^2 = 0.9913, n = 6) (Fig. 5B). The limit of detection (LOD) value of the fluorometric biosensor

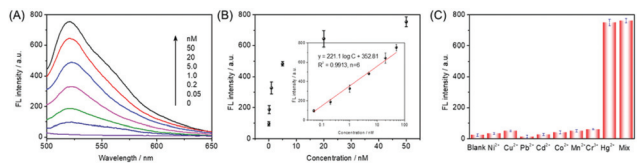

Fig. 5 (A) The fluorescence intensity responses of Ti_3C_2-based Hg^{2+}-induced Exo III-assisted target recycling fluorometric strategy toward various concentrations of Hg^{2+} (0, 0.05, 0.2, 1.0, 5.0, 20, and 50 nM). (B) Calibration plots corresponding to peak fluorescence intensity (at 520 nm) as a function of Hg^{2+} concentration (nM). (C) The anti-interference ability against Hg^{2+} (50 nM) and seven coexisting metal ions (500 nM), namely Ni^{2+}, Cu^{2+}, Pb^{2+}, Cd^{2+}, Co_2^{+}, Mn^{2+}, Cr^{3+} (note: all these metal ions are included in the mixture). The blank sample indicates the use of deionized water instead of the sample containing metal ions.

was estimated to be 42.5 pM in terms of the 3δ-rule (note: δ represents the standard deviation for 11-blank fluorescence response), which was significantly lower than that of existing Hg^{2+} detection strategies (Table 1). The relative standard deviation (n = 3) values were 1.25%, 2.83% and 3.42% for intra-assays and 5.81%, 6.53% and 6.11% for inter-assays toward high-middle-low Hg^{2+} concentrations (0.05, 5.0 and 50 nM), respectively, undoubtedly demonstrating good reproducibility and ideal accuracy.

The specificity of the Ti_3C_2-based Hg^{2+}-induced Exo III-assisted target recycling fluorometric system was further systematically investigated with the intervention of seven coexisting interfering metal ions (500 nM), namely Ni^{2+}, Cu^{2+}, Pb^{2+}, Cd^{2+}, Co_2^{+}, Mn^{2+}, and Cr^{3+}, under the same experimental conditions. These high-concentration (10 times that of the analyte) non-target metal ions showed no obvious variation of fluorescence intensity responses in comparison with the blank sample (deionized water), while the fluorescence intensities of Hg^{2+} and mixtures containing Hg^{2+} increased apparently (Fig. 5C), showing the satisfactory discrimination ability for the analyte Hg^{2+}.

Detection of Hg^{2+} from real environment samples

To demonstrate the possibility of the manufactured Ti_3C_2-based Hg^{2+}-induced Exo III-assisted target recycling fluorometric strategy for practical applications, we performed Hg^{2+} concentration analysis and recovery experiments by testing environmental samples (tap water and river water). Hg^{2+} standards with different concentrations (0.2, 5.0, 20 nM) were first spiked in blank water samples. The obtained spiked samples were determined by the proposed fluorometric strategy and the Hg^{2+} concentration was obtained through the regression equation (Fig. 5B). The acceptable recovery rates (95.0%–

Table 2 Detection of Hg^{2+} in different water samples using the fluorometric biosensor

Sample	Added Hg^{2+} (nM)	Measured (mean ± SD, ng mL^{-1}, n = 3)	Recovery (%)
Tap water	0.2	0.19 ± 0.05	95.0
	5.0	5.09 ± 0.09	101.8
	20	20.62 ± 0.18	103.1
River water	0.2	0.22 ± 0.09	110
	5.0	4.91 ± 0.11	98.2
	20	19.8 ± 0.22	96.9

Table 1 Comparison of analytical properties of different Hg^{2+}-based schemes

Transduced signal	Dynamic range (nM)	LOD (nM)	Ref.
Polyethylenimine/glutathione fluorometric biosensor	100–100 000	32	26
Nitrogen-doped graphene quantum dots fluorometric assay	2–200	0.32	27
Carbon dots/cadmium telluride fluorometric assay	10–1400	4600	28
L-Cysteine-modified gold nanoparticles fluorometric assay	2–30 000	1.3	29
AuNP@β-CD aggregation-based photothermometric	400–8000	60	30
Covalent organic framework/gold nanoparticles colorimetric	5–300	0.75	31
Exo III-assisted recycling Ti_3C_2 fluorometric biosensor	0.05–50	0.0425	This work

103.1%; Table 2) indicated that the proposed fluorometric biosensor provided a promising potential for the analysis of complex environmental water samples with great accuracy and reliability.

Conclusions

This contribution describes a facile fluorometric bioanalysis platform for the rapid determination of Hg^{2+} by using ultrathin two-dimensional MXenes (Ti_3C_2) as fluorescence quencher and Hg^{2+}-induced Exo III-assisted recycling for efficient signal amplification. On the one hand, Ti_3C_2 is a strong fluorescence quencher for fluorescent dyes; on the other hand, it has obvious distinguishability for ssDNA and dsDNA. Such versatility and promising properties mean that Ti_3C_2 can act as sensing material in molecular diagnostics and fluorescence sensing. Coupling Ti_3C_2 nanosheets with Exo III-assisted multiple recycling strategy, this fluorometric platform showed improved sensitivity with a LOD of 42.5 pM. Furthermore, the anti-interference of the constructed fluorometric strategy was ensured by the specific T-Hg^{2+}-T interaction, which can distinguish Hg^{2+} from other possible background metal ions. Additionally, the detection process is a homogeneous mix-and-detect one with simplified operation, which makes it possible to develop simple, robust and sensitive molecular diagnostic tools. This contribution not only expands the distinct application of Ti_3C_2 in a fluorometric DNA biosensor, but also paves the way for other two-dimensional materials to design advanced biosensing/biomedical systems (controlled delivery of nucleic acids or nanopore-based biomolecule detection).

Conflicts of interest

There are no conflicts to declare.

Acknowledgements

The authors acknowledge financial support from the National Natural Science Foundation of China (grant no. 21874022 and 21675029).

References

1 M. Zhao, C. Ren, Z. Ling, M. Lukatskaya, C. Zhang, A. Van, M. Barsoum and Y. Gogotsi, *Adv. Mater.*, 2015, **27**, 339–345.
2 M. Ghidiu, M. Lukatskaya, M. Zhao, Y. Gogotsi and M. Barsoum, *Nature*, 2014, **516**, 78–81.
3 A. Dillon, M. Ghidiu, A. Krick, J. Griggs, S. May, Y. Gogotsi, M. Barsoum and A. Fafarman, *Adv. Funct. Mater.*, 2016, **26**, 4162–4168.
4 M. Naguib, J. Halim, J. Lu, K. Cook, L. Hultman, Y. Gogotsi and M. Barsoum, *J. Am. Chem. Soc.*, 2013, **135**, 15966–15969.
5 K. Huang, Z. Li, J. Lin, G. Han and P. Huang, *Chem. Soc. Rev.*, 2018, **47**, 5109–5124.
6 C. Dai, H. Lin, G. Xu, Z. Liu, R. Wu and Y. Chen, *Chem. Mater.*, 2017, **29**, 8637–8652.
7 Y. Wen, T. Rufford, X. Chen, N. Li, M. Lyu, L. Dai and L. Wang, *Nano Energy*, 2017, **38**, 368–376.
8 M. Okubo, A. Sugahara, S. Kajiyama and A. Yamada, *Acc. Chem. Res.*, 2018, **51**, 591–599.
9 Q. Zhang, F. Wang, H. Zhang, Y. Zhang, M. Liu and Y. Liu, *Anal. Chem.*, 2018, **90**, 12737–12744.
10 M. Mojtabavi, A. VahidMohammadi, W. Liang, M. Beidaghi and M. Wanunu, *ACS Nano*, 2019, **13**, 3042–3053.
11 J. Zheng, B. Wang, Y. Jin, B. Weng and J. Chen, *Microchim. Acta*, 2019, **186**, 95.
12 C. Lorena Manzanares-Palenzuela, A. Pourrahimi, J. Gonzalez-Julian, Z. Sofer, M. Pykal, M. Otyepka and M. Pumera, *Chem. Sci.*, 2019, **10**, 10010–10017.
13 X. Peng, Y. Zhang, D. Lu, Y. Guo and S. Guo, *Sens. Actuators, B*, 2019, **281**, 445–452.
14 Z. Huang, B. Liu and J. Liu, *Langmuir*, 2019, **35**, 9858–9866.
15 Y. Gerasimova and D. Kolpashchikov, *Chem. Soc. Rev.*, 2014, **43**, 6405–6438.
16 R. Zeng, Z. Luo, L. Zhang and D. Tang, *Anal. Chem.*, 2018, **90**, 12299–12306.
17 R. Zeng, Z. Luo, L. Su, L. Zhang, D. Tang, R. Niessner and D. Knopp, *Anal. Chem.*, 2019, **91**, 2447–2454.
18 Y. Zhou, B. Li, M. Wang, J. Wang, H. Yin and S. Ai, *Microchim. Acta*, 2017, **184**, 4359–4365.
19 W. Ren, Y. Zhang, H. Chen, Z. Gao, N. Li and H. Luo, *Anal. Chem.*, 2016, **88**, 1385–1390.
20 Y. Zhang, L. Tang, F. Yang, Z. Sun and G. Zhang, *Microchim. Acta*, 2015, **182**, 1535–1541.
21 J. Chen, S. Zhou and J. Wen, *Anal. Chem.*, 2014, **86**, 3108–3114.
22 J. Joseph and A. Anappara, *J. Lumin.*, 2017, **192**, 761–766.
23 C. Driscoll, R. Mason, H. Chan, D. Jacob and N. Pirrone, *Environ. Sci. Technol.*, 2013, **47**, 4967–4983.
24 R. Zhang, L. Deng, P. Zhu, S. Xu, C. Huang, Y. Zeng, S. Ni and X. Zhang, *Microchim. Acta*, 2017, **184**, 541–546.
25 G. Cai, Z. Yu, P. Tong and D. Tang, *Nanoscale*, 2019, **11**, 15659–15667.
26 D. Luo, S. Liu, N. Li and H. Luo, *Microchim. Acta*, 2018, **185**, 6.
27 D. Peng, L. Zhang, R. Liang and J. Qiu, *ACS Sens.*, 2018, **3**, 1040–1047.
28 E. Ghasemi, M. R. Hormozi-Nezhad and M. Mahmoudi, *Sens. Actuators, B*, 2018, **259**, 894–899.
29 X. Ma, Z. Wang and S. He, *Microchim. Acta*, 2019, **186**, 632.
30 P. An, H. Rao, M. Gao, X. Xue, X. Liu, X. Lu and Z. Xue, *Chem. Commun.*, 2020, **56**, 9799–9802.
31 W. Li, Y. Li, H. Qian, X. Zhao, C. Yang and X. Yan, *Talanta*, 2019, **204**, 224–228.